A nanoluciferase SARS-CoV-2 for rapid neutralization testing and screening of anti-infective drugs for COVID-19

Xuping Xie[1,#,*], Antonio E. Muruato[1,2,#], Xianwen Zhang[1], Kumari G. Lokugamage[2], Camila R. Fontes-Garfias[1], Jing Zou[1], Jianying Liu[2], Ping Ren[3], Mini Balakrishnan[4], Tomas Cihlar[4], Chien-Te K. Tseng[2], Shinji Makino[2], Vineet D. Menachery[2,3,5], John P. Bilello[4*], and Pei-Yong Shi[1,5,6,7*]

[1]Department of Biochemistry and Molecular Biology, University of Texas Medical Branch, Galveston TX, USA

[2]Department of Microbiology and Immunology, University of Texas Medical Branch, Galveston TX, USA

[3]Department of Pathology, University of Texas Medical Branch, Galveston TX, USA

[4]Gilead Sciences, Inc., Foster City, CA, USA

[5]Institute for Human Infections and Immunity, University of Texas Medical Branch, Galveston, TX, USA

[6]Sealy Institute for Vaccine Sciences, University of Texas Medical Branch, Galveston, TX, USA

[7]Sealy Center for Structural Biology & Molecular Biophysics, University of Texas Medical Branch, Galveston, TX, USA

[#]X.X. and A.E.M. contributed equally to this study

*Correspondence: X.X. (xuxie@UTMB.edu), J.P.B. (john.bilello@gilead.com), or P.-Y.S. (peshi@UTMB.edu)

Running title: A rapid neutralization assay and screen of anti-infective drugs for COVID-19

Keywords: SARS-CoV-2, COVID-19, serological diagnosis, vaccine, antiviral, drug repurpose, coronavirus

Abstract

A high-throughput platform would greatly facilitate COVID-19 serological testing and antiviral screening. Here we report a nanoluciferase SARS-CoV-2 (SARS-CoV-2-Nluc) that is genetically stable and replicates similarly to the wild-type virus in cell culture. We demonstrate that the optimized reporter virus assay in Vero E6 cells can be used to measure neutralizing antibody activity in patient sera and produces results in concordance with a plaque reduction neutralization test (PRNT). Compared with the low-throughput PRNT (3 days), the SARS-CoV-2-Nluc assay has substantially shorter turnaround time (5 hours) with a high-throughput testing capacity. Thus, the assay can be readily deployed for large-scale vaccine evaluation and neutralizing antibody testing in humans. Additionally, we developed a high-throughput antiviral assay using SARS-CoV-2-Nluc infection of A549 cells expressing human ACE2 receptor (A549-hACE2). When tested against this reporter virus, remdesivir exhibited substantially more potent activity in A549-hACE2 cells compared to Vero E6 cells (EC_{50} 0.115 vs 1.28 μM), while this difference was not observed for chloroquine (EC_{50} 1.32 vs 3.52 μM), underscoring the importance of selecting appropriate cells for antiviral testing. Using the optimized SARS-CoV-2-Nluc assay, we evaluated a collection of approved and investigational antivirals and other anti-infective drugs. Nelfinavir, rupintrivir, and cobicistat were identified as the most selective inhibitors of SARS-CoV-2-Nluc (EC_{50} 0.77 to 2.74 μM). In contrast, most of the clinically approved antivirals, including tenofovir alafenamide, emtricitabine, sofosbuvir, ledipasvir, and velpatasvir were inactive at concentrations up to 10 μM. Collectively, this high-throughput platform represents a reliable tool for rapid neutralization testing and antiviral screening for SARS-CoV-2.

Introduction

Severe acute respiratory syndrome coronavirus 2 (SARS-CoV-2) emerged in Wuhan, China in late 2019[1,2] and caused global pandemic of coronavirus disease 2019 (COVID-19). Two other human coronaviruses emerged in the past two decades and caused severe respiratory syndrome, including SARS-CoV in 2002 and Middle East respiratory syndrome (MERS-CoV) in 2012[3]. In addition, four endemic human coronaviruses (*i.e.*, OC43, 229E, NL63, and HKU1) cause common cold respiratory diseases. For COVID-19 diagnosis, nucleic acid-based RT-PCR assays have been used to identify individuals with acute viral infection. The RT-PCR assay is essential for detecting and contact tracing to control viral transmission. Given the unknown extent of asymptomatic infections, rapid and reliable serological assays are urgently needed to determine the real scale of local community infections. In addition, the ability to quickly measure neutralizing antibody levels is required to determine the protective immunity of previously infected individuals, to identify convalescent donors with protective antibodies for plasma therapy, and to evaluate various vaccines under development. Although various serological assay platforms have been developed [*e.g.*, lateral flow immunoassay, ELISA, microsphere immunoassay, and vesicular stomatitis virus (VSV) pseudotyped with SARS-CoV-2 spike], the conventional plaque reduction neutralization test (PRNT) remains the gold standard of serological diagnosis because it directly measures the neutralizing antibody levels required to block an authentic viral infection. However, the low throughput and long assay turnaround time make PRNT impossible for large scale diagnosis, representing a critical gap for COVID-19 response and countermeasure development.

The goals of this study were to (i) develop a rapid neutralization assay that maintains the gold standard of PRNT for serological COVID-19 diagnosis, (ii) establish a high-throughput assay for reliable antiviral screening, and (ii) screen exploratory and FDA-approved anti-infective drugs for potential COVID-19 repurposing. We established a nanoluciferase SARS-CoV-2 (SARS-CoV-2-Nluc) as a platform for rapid serodiagnosis and high-throughput drug

screening. When used to test COVID-19 patient sera, the rapid neutralization assay yielded results commensurate with the conventional PRNT. A version of the SARS-CoV-2-Nluc infection assay has also been developed for high throughput screening of antivirals and validated using known SARS-CoV-2 inhibitors such as remdesivir and chloroquine. The developed assay was employed to test a collection of approved and investigational anti-infective drugs, including established antivirals against HIV and HCV.

Results

A stable SARS-CoV-2-Nluc. Using an infectious cDNA clone of SARS-CoV-2 (strain 2019-nCoV/USA_WA1/2020)[4], we engineered nanoluciferase (Nluc) gene at the OFR7 of the viral genome (Fig. 1a). Seven cDNA fragments spanning the SARS-CoV-2 genome were ligated *in vitro* to generate a full-genome Nluc cDNA. A T7 promoter was engineered to *in vitro* transcribe the full-length Nluc viral RNA. The RNA transcript was highly infectious after electroporation into Vero E6 cells (African green monkey kidney epithelial cells), producing 10^7 PFU/ml of virus. The infectious clone-derived SARS-CoV-2-Nluc developed plaques slightly larger than the wild-type recombinant SARS-CoV-2 (Fig. 1b). The SARS-CoV-2-Nluc and wild-type SARS-CoV-2 exhibited similar replication kinetics in Vero E6 cells (Fig. 1c), indicating that insertion of Nluc gene does not affect the viral replication *in vitro*.

To examine the stability of SARS-CoV-2-Nluc, we continuously cultured the virus for five passages on Vero E6 cells (1-2 days per passage). The passage 5 (P5) virus produced similar plaque morphology (Fig. 1d), replication kinetics (Fig. 1e), and luciferase profile as the P1 virus (Fig. 1f). Next, we performed RT-PCR to verify the retention of Nluc gene in the P1 and P5 viral genomes using two primers spanning the insertion junctions (nucleotides 25,068-28,099 of viral genome). The RT-PCR products derived from both P1 and P5 SARS-CoV-2-Nluc were 156-bp larger than that from the wild-type recombinant SARS-CoV-2 (Fig. 1g, lanes 1-3). The 156-bp

difference is due to the substitution of ORF7 (368 bp) with Nluc gene (513 bp). Digestion of the RT-PCR products with BsrGI (located upstream of the Nluc insertion) and PacI (located at the C-terminal region of Nluc) generated distinct DNA fragments between the Nluc and wild-type viruses, whereas the P1 and P5 viruses produced identical digestion patterns (Fig. 1g, lanes 4-6). Furthermore, we confirmed the retention of Nluc reporter by sequencing the P1 and P5 RT-PCR products (Fig. 1h). Compared with the infectious clone-derived wild-type SARS-CoV-2[4], both P1 and P5 reporter viruses contained five single nucleotide mutations that led to amino acid changes in different viral proteins (Fig. 1h). These mutations may account for the slightly larger plaques of SARS-CoV-2-Nluc. No other mutations were recovered from the passaged viruses. Altogether, the results demonstrate that SARS-CoV-2-Nluc stably maintains the reporter gene after five rounds of passaging on Vero E6 cells.

Human angiotensin-converting enzyme (hACE2) as a receptor for SARS-CoV-2. We explored SARS-CoV-2-Nluc to study virus entry, serological diagnosis, and antiviral screening. Infection of Vero E6 cells with SARS-CoV-2-Nluc [multiplicity of infection (MOI) 1.0] produced a robust Nluc profile that peaked at 24 h post-infection (p.i.; Fig. 2a). As early as 1 h p.i., the Nluc signal was >10 fold above the background, suggesting that Nluc signals at early timepoints may be used to study virus entry. Thus, we evaluated the function of hACE2 in virus entry by pre-incubating Vero E6 cells with anti-hACE2 polyclonal antibodies for 1 h, followed by SARS-CoV-2-Nluc infection (Fig. 2b). The anti-hACE2 antibodies inhibited Nluc signal at 6 h p.i. in a dose-responsive manner (Fig. 2c). As a negative control, pre-treatment with antibodies against hDPP4 (a receptor for MERS-CoV infection) did not suppress Nluc activity (Fig. 2c), indicating the role of hACE2 in SARS-CoV-2 entry. To further evaluate these results, we compared the efficiencies of virus entry between naïve A549 (a human alveolar epithelial cell line) and A549 stably expressing hACE2 (A549-hACE2; Fig. 2d). At various MOIs, the Nluc signals (collected at 24 h p.i.) from A549-hACE2 cells were ~100-fold higher than those from the

naïve A549 cells (Fig. 2e). Collectively, the results support hACE2 as a receptor for SARS-COV-2 entry.

A rapid neutralization assay for COVID-19 diagnosis. The robust early Nluc signals after SARS-COV-2-Nluc infection (Fig. 2a) prompted us to develop a rapid neutralization assay. Fig. 3a depicts the flowchart of SARS-COV-2-Nluc neutralization assay in a 96-well format. After incubating serum samples with SARS-COV-2-Nluc at 37°C for 1 h, the virus/serum mixtures were added to Vero E6 cells (pre-seeded in a 96-well plate) at an MOI of 0.5. At 4 h p.i., Nluc signals were measured to determine the serum dilution that neutralized 50% of Nluc activity (NT_{50}). We chose 4 h p.i. as the assay end time because the Nluc signal at this timepoint was >100 fold above the background (Fig. 2a). The total assay time to completion was 5 h (1 h virus/serum incubation plus 4 h viral infection). Following this protocol, we tested twenty-one COVID-19-positive sera from RT-PCR-confirmed patients and nine COVID-19-negative human sera (collected before COVID-19 emergence; Fig. 3b). All COVID-19-positive sera (samples 1-21) showed positive NT_{50} of 66 to 7237, while all COVID-19-negative sera (samples 22-30) showed negative NT_{50} <20, the lowest tested serum dilution. Fig. 3c shows three representative neutralization curves: Nluc signals were suppressed by the positive sera in an inverse dilution-dependent manner. The results suggest that SARS-COV-2-Nluc could be used for rapid neutralization testing.

To validate the Nluc neutralization results, we performed conventional PRNT on the same set of patient sera. The twenty-one COVID-19-positive samples exhibited $PRNT_{50}$ of 80 to 3200, and the nine COVID-19-negative samples showed $PRNT_{50}$ <20 (Fig. 3b). The neutralization results between the Nluc virus and PRNT assays had a correlation coefficient (R^2) of 0.8395 (Fig. 3d). Notably, the NT_{50} values from the Nluc assay are on average 3-fold higher than the $PRNT_{50}$ values form the plaque assay. Overall, the results indicate that the SARS-CoV-

2-Nluc neutralization assay detects neutralizing antibodies in COVID-19 patient sera with a higher sensitivity than the conventional PRNT assay.

A high-throughput antiviral assay for SARS-CoV-2. Reporter viruses have been commonly used for antiviral screening[5-11]. Therefore, we developed a 96-well format antiviral assay using the SARS-CoV-2-Nluc reporter virus. Vero E6 cells were initially used in our assay development because this cell line is highly susceptible to SARS-CoV-2 infection[1]. Since COVID-19 is a respiratory disease, we also tested A549 (a human alveolar epithelial cell line) for the assay development. However, due to the low permissiveness of A549 for SARS-CoV-2-Nluc infection, we included A549-hACE2 cells to enhance viral infection in our assay (Fig. 2e). Two SARS-CoV-2 inhibitors that received the emergency use authorization in US for COVID-19 at the time of assay development, chloroquine phosphate (a malaria drug) and remdesivir (an antiviral adenosine analog prodrug)[12], were used to evaluate the assay in both Vero E6 and A549-hACE2 cells (Fig. 4). In a 3-day cytotoxicity assay, chloroquine showed CC_{50} of >50 μM on both cells, whereas remdesivir had CC_{50} of >50 μM and 32.5 μM in Vero E6 and A549-hACE2 cells, respectively (Fig. 4a,b). For testing antiviral activity, we optimized the assay conditions (12,000 Vero or A549-hACE2 cells per well and MOI 0.025) to allow for multiple rounds of viral replication in 48 h p.i. without developing significant cytopathic effect (CPE). Both chloroquine and remdesivir inhibited Nluc activity in a dose-dependent manner (Fig. 4c,d). Importantly, the EC_{50} value for remdesivir in A549-hACE2 cells (0.115 μM) was >10-fold lower than that in Vero E6 cells (1.28 μM), while the potency of chloroquine was only marginally different between the two cell lines (EC_{50} 1.32 vs 3.52 μM; Fig. 4e). This result underscores the importance of using biologically relevant cells for antiviral testing. Thus, we chose A549-hACE2 for the following high-throughput antiviral screening of additional compounds.

Testing of clinically relevant anti-infective drugs for antiviral activity against SARS-CoV-2. A broad selection of forty clinically approved and investigational antivirals and

other anti-infective drugs were tested for anti-SARS-CoV-2-Nluc activities in A549-hACE2 cells. Based on their indication and/or mode of action, the tested drugs belong to four categories, including (i) antiviral nucleoside/nucleotide analogs, (ii) HIV antivirals, (iii) HCV antivirals, and (iv) other primarily anti-infective drugs.

(i) Nucleoside/nucleotide analog drugs. Ten nucleoside analogs with antiviral activities against other viruses were evaluated for activity against SARS-CoV-2-Nluc (Table 1). Only remdesivir showed SARS-CoV-2-Nuc activity with an EC_{50} and CC_{50} of 0.115 and 32.7 µM, respectively, and selectivity index (SI = CC_{50}/EC_{50}) of 284. No other nucleoside analogs, including sofosbuvir or any other 2'C-methyl substituted anti-HCV nucleosides or their prodrugs, exhibited anti-SARS-CoV-2 activity at concentrations up to 10 µM. The results agree with previous reports demonstrating potent inhibition of SARS-CoV-2 by remdesivir in physiologically relevant airway epithelial cells[13], and lack of SARS-CoV-2 inhibition by favipiravir and/or ribavirin[14-16].

(ii) HIV antivirals. Fifteen clinically approved antiretrovirals, including protease inhibitors (PIs), nucleoside/nucleotide reverse-transcriptase inhibitors (NRTIs), non-nucleoside reverse transcriptase inhibitors (NNRTIs), and an integrase strand-transfer inhibitor (INSTI), were assessed for their activities against SARS-CoV-2-Nluc (Table 2). Among the nine FDA-approved HIV PIs tested, nelfinavir was the only compound that inhibited SARS-CoV-2-Nluc with a sub-micromolar potency (EC_{50} 0.77 µM), albeit with a relatively narrow SI of 16. Factoring in human plasma protein binding of nelfinavir[17], the projected protein adjusted potency ($paEC_{50}$ ~30 µM) is significantly above the clinically achievable plasma concentration of the drug (Table 2). Of the remaining PIs, five were inactive (amprenavir, ritonavir, indinavir, darunavir, and atazanavir with EC_{50} >10 µM) and three exhibited rather weak antiviral activity (lopinavir, saquinavir, and tipranavir with EC_{50} of 8-9 µM and SI of 3-4).

Among the HIV RT inhibitors, all three NRTIs (emtricitabine, tenofovir alafenamide, and rovafovir) were inactive against SARS-CoV-2-Nluc with EC_{50} >10 µM (Table 2). The two

NNRTIs (rilpivirine and efavirenz) exhibited poor SI <3.9. Bictegravir, a drug targeting HIV integrase, was inactive against SARS-CoV-2-Nluc with EC_{50} >10 µM (Table 2).

(iii) HCV antivirals. Nine FDA-approved HCV drugs with diverse modes of action targeting viral protease, polymerase (both nucleotide and non-nucleoside inhibitors), or NS5A protein were tested. None of them showed any anti-SARS-CoV-2-Nluc activities with EC_{50} >10 µM (Table 3).

(iv) Other classes of drugs. Ten additional clinically validated drugs, six of which are anti-infective medicines, were tested against SARS-CoV-2-Nluc (Table 4). Rupintrivir, a human rhinovirus (HRV) 3CLpro cysteine protease inhibitor, inhibited SARS-CoV-2-Nluc with EC_{50} 1.87 µM, representing a 156-fold lower potency than that against HRV[18]. Niclosamide (an antihelminthic drug) showed anti-SARS-COV-2-Nluc activity (EC_{50} 0.715 µM) with low selectivity (SI 1.8). As described in Fig. 4, chloroquine exhibited selective inhibition of anti-SARS-CoV-2-Nluc (EC_{50} 1.32 µM and SI >37.9). Presatovir, a respiratory syncytial virus (RSV) fusion inhibitor, showed an EC_{50} of 2.53 µM and SI of >37.9. The EC_{50} of presatovir against SARS-CoV-2 is 7,000-fold less potent than against RSV[19], establishing that clinical exposures are below the EC_{50} determined for SARS-CoV-2[20], precluding the potential for COVID-19 therapy. Cobicistat, a selective mechanism-based inhibitor of CYP3A enzymes, weakly inhibited SARS-CoV-2-Nluc (EC_{50} 2.7 µM) with a modest SI of 17.3. Oseltamavir carboxylate and baloxavir, two approved drugs targeting influenza A virus neuraminidase and endonuclease, respectively, were inactive against SARS-CoV-2-Nluc with EC_{50} >10 µM. Nivocasan, an inhibitor of cellular caspases 1, 8, and 9 (treatment for hepatic fibrosis and non-alcoholic steatohepatitis related to HCV infection), as well as two inhibitors of Bruton's tyrosine kinase (BTK; treatment for lymphoma and leukemia) were also inactive against SARS-CoV-2 with EC_{50} >10 µM (Table 4). Taken together, only remdesivir, chloroquine, and rupintrivir have antiviral activity against recombinant SARS-CoV-2-Nluc.

Discussion

We developed a stable reporter SARS-CoV-2-Nluc variant for rapid neutralization testing. Since neutralizing titer is a key parameter to predict immunity, the rapid SARS-CoV-2-Nluc neutralization assay will enable many aspects of COVID-19 research, including epidemiological surveillance, vaccine development, and antiviral discovery. Although the current assay was performed in a 96-well format, given the magnitude and dynamic range of Nluc signal, it can be readily adapted to a 384- or 1536-well format for large-scale testing. Notably, when diagnosing patient sera, the SARS-CoV-2-Nluc assay generated NT_{50} value on average 3-fold higher than the conventional $PRNT_{50}$. The higher sensitivity of the SARS-CoV-2-Nluc assay might be due to different endpoint readouts (plaque counts versus luminescence signal of Nluc that could accumulate in cells). Importantly, compared with the conventional PRNT assay, our reporter neutralization test has shortened the turnaround time from 3 days to 5 h and increased the testing capacity. Despite the strengths of high throughput and speed, the current rapid neutralization assay must be performed in a biosafety level 3 (BSL-3) facility, representing a major limitation. Experiments are ongoing to attenuate SARS-CoV-2-Nluc so that the assay could be performed in a BSL-2 laboratory. Aligned with the same premise, BSL-2 lab compatible neutralization assays have been reported using VSV pseudotyped with SARS-CoV-2 spike protein[21,21].

We additionally optimized and validated the recombinant SARS-CoV-2-Nluc for high-throughput antiviral screening. Our results demonstrate that cell type could significantly affect a compound's EC_{50} value, underscoring the importance of using biologically relevant cells for drug discovery. The extent of EC_{50} discrepancy from different cells was dependent on the compound's mode of action. Remdesivir EC_{50} values differed by >10-fold when the assay used Vero E6 and A549-hACE2 cells. In another study, remdesivir was shown to be even more potent (EC_{50} 0.01 μM) when tested on primary human airway epithelial (HAE) cells[13]. The potency differences seen between cell types are due to the differential metabolism of remdesivir

in various cells. Host metabolic enzymes are required to convert the remdesivir prodrug to a monophosphate substrate, which is further metabolized by host kinases to its active triphosphate form that incorporates into viral RNA for chain termination. Vero E6 cells are less efficient in forming the active triphosphate than A549-hACE2 and primary HAE cells[13,22], leading to higher EC_{50} values. The antiviral activity of chloroquine was more consistent between the two cell lines tested, indicating that its mode of action is independent of host metabolism. This highlights the need for careful and appropriate interpretation of *in vitro* antiviral data for compounds with different mechanisms of action such as remdesivir and chloroquine, which may appear similar in some cell types but are substantially different in cells that are more clinically relevant for SARS-CoV-2 infection.

Remdesivir has received the FDA EUA for COVID-19 treatment and is being tested in additional clinical trials, including combination therapies. In a double-blind, randomized, placebo-controlled trial involving 1,063 patients hospitalized with COVID-19, patients receiving remdesivir experienced a shortened recovery time of 11 days as compared with 15 days for patients in the placebo group[23]. Besides SARS-CoV-2, remdesivir was also shown to potently inhibit SARS-CoV and MERS-CoV in cell culture and animal models[13,24-27]. For chloroquine, inconsistent results were obtained from several clinical studies with small patient numbers[28-30]. A recent retrospective multicenter study involving >1,400 patients showed that treatment with hydroxychloroquine, azithromycin, or both, compared with no treatment, was not associated with significant differences in fatality rate among hospitalized patients[31]. These and other controversial results prompted recent decision by FDA to revoke the EUA for chloroquine and hydroxychloroquine (https://www.fda.gov/news-events/press-announcements/coronavirus-covid-19-update-fda-revokes-emergency-use-authorization-chloroquine-and).

Using the validated SARS-CoV-2-Nluc/A549-hACE2 infection assay, we screened a collection of 40 clinically relevant antivirals and anti-infective drugs. In addition to remdesivir and

chloroquine used for the assay validation, nelfinavir (HIV protease inhibitor), rupintrivir (HRV protease inhibitor), and cobicistat (a pharmacoenhancer and inhibitor of CYP450) were identified as the most potent and selective inhibitors among the tested compounds with EC_{50} values ranging from 0.77 to 2.74 µM and SI >15-fold. In studies with HIV *in vitro*, a 40-fold shift in the antiviral EC_{50} was reported when assays were conducted in the presence of 50% human serum[17], an effect also likely relevant for COVID-19. Based on their antiviral potencies established in vitro, it is unlikely that nelfinavir or cobicistat would exert major clinical effects in COVID-19 patients at the current clinically approved doses, since their systemic free drug levels based on total plasma concentration and established plasma protein binding are below their measured *in vitro* EC_{50} for SARS-CoV-2-Nluc[39,45]. Rupintrivir is a selective covalent inhibitor of HRV 3CLpro cysteine protease[18], and thus may inhibit SARS-CoV-2 through blocking the main 3CLpro cysteine protease activity. Rupintrivir has potent activity *in vitro* against HRV that is approximately 100-fold better compared to SARS-CoV-2[32]. It has been tested clinically as an intranasal spray for the treatment of HRV-associated common cold[33], but there is no clinical experience with either systemic or inhaled administration of rupintrivir. Hence, further studies would be required to better understand rupintrivir's mode of action, efficacy in animal models, and potential clinical benefits in COVID-19 patients depending on the route of administration.

Several antiviral drugs approved for the treatment of HIV or HCV have been suggested to be potentially useful for the treatment of COVID-19[34,35]. These include in particular, sofosbuvir either alone[35,36] or in combination with velpatasvir[37], in addition to HIV NNRTIs tenofovir[38] and emtricitabine[34,35]. Their activities against SARS-CoV-2 were postulated primarily based on computational modeling of their interactions with the viral RdRp. Our results clearly demonstrate the lack of antiviral activity of this group of drugs against SARS-CoV-2; therefore, these drugs do not justify clinical studies in COVID-19 patients.

In summary, we have developed a stable recombinant SARS-CoV-2-Nluc for use in rapid neutralization testing and high-throughput antiviral drug discovery. Using the optimized and validated high-throughput infection assay, we screened a collection of approved and investigational antivirals and other anti-infective drugs. Among the tested agents, rupintrivir was identified as a selective *in vitro* inhibitor of SARS-CoV-2 that might be considered for further studies to fully establish its potential for the treatment of COVID-19.

References

1 Zhou, P. *et al.* A pneumonia outbreak associated with a new coronavirus of probable bat origin. *Nature* **579**, 270-273, doi:10.1038/s41586-020-2012-7 (2020).

2 Zhu, N. *et al.* A Novel Coronavirus from Patients with Pneumonia in China, 2019. *N Engl J Med* **382**, 727-733, doi:10.1056/NEJMoa2001017 (2020).

3 de Wit, E., van Doremalen, N., Falzarano, D. & Munster, V. J. SARS and MERS: recent insights into emerging coronaviruses. *Nat Rev Microbiol* **14**, 523-534, doi:10.1038/nrmicro.2016.81 (2016).

4 Xie, X. *et al.* An Infectious cDNA Clone of SARS-CoV-2. *Cell Host Microbe* **27**, 841-848 e843, doi:10.1016/j.chom.2020.04.004 (2020).

5 Puig-Basagoiti, F. *et al.* High-throughput assays using luciferase-expressing replicon, virus-like particle, and full-length virus for West Nile virus drug discovery. *Antimicrob. Agent. Chemother.* **49**, 4980-4988 (2005).

6 Zou, G., Xu, H. Y., Qing, M., Wang, Q. Y. & Shi, P. Y. Development and characterization of a stable luciferase dengue virus for high-throughput screening. *Antiviral Res* **91**, 11-19, doi:10.1016/j.antiviral.2011.05.001 (2011).

7 Shan, C. *et al.* An Infectious cDNA Clone of Zika Virus to Study Viral Virulence, Mosquito Transmission, and Antiviral Inhibitors. *Cell Host Microbe* **19**, 891-900, doi:10.1016/j.chom.2016.05.004 (2016).

8 Scobey, T. *et al.* Reverse genetics with a full-length infectious cDNA of the Middle East respiratory syndrome coronavirus. *Proc Natl Acad Sci U S A* **110**, 16157-16162, doi:10.1073/pnas.1311542110 (2013).

9 Almazan, F. *et al.* Coronavirus reverse genetic systems: infectious clones and replicons. *Virus Res* **189**, 262-270, doi:10.1016/j.virusres.2014.05.026 (2014).

10 Hou, Y. J. *et al.* SARS-CoV-2 Reverse Genetics Reveals a Variable Infection Gradient in the Respiratory Tract. *Cell* **182**, 1–18 (2020).

11 Roberts, R. S., Yount, B. L., Sims, A. C., Baker, S. & Baric, R. S. Renilla luciferase as a reporter to assess SARS-CoV mRNA transcription regulation and efficacy of anti-SARS-CoV agents. *Adv Exp Med Biol* **581**, 597-600, doi:10.1007/978-0-387-33012-9_108 (2006).

12 Wang, M. *et al.* Remdesivir and chloroquine effectively inhibit the recently emerged novel coronavirus (2019-nCoV) in vitro. *Cell Res* **30**, 269-271, doi:10.1038/s41422-020-0282-0 (2020).

13 Pruijssers, A. J. *et al.* Remdesivir potently inhibits SARS-CoV-2 in human lung cells and chimeric SARS-CoV expressing the SARS-CoV-2 RNA polymerase in mice. *bioRxiv* **doi:** https://doi.org/10.1101/2020.04.27.064279 (2020).

14 Choy, K. T. *et al.* Remdesivir, lopinavir, emetine, and homoharringtonine inhibit SARS-CoV-2 replication in vitro. *Antiviral Res* **178**, 104786, doi:10.1016/j.antiviral.2020.104786 (2020).

15 Jeon, S. *et al.* Identification of antiviral drug candidates against SARS-CoV-2 from FDA-approved drugs. *Antimicrob Agents Chemother*, doi:10.1128/AAC.00819-20 (2020).

16 Liu, J. *et al.* A 2'-deoxy-2'-fluoro-2'-C-methyl uridine cyclopentyl carbocyclic analog and its phosphoramidate prodrug as inhibitors of HCV NS5B polymerase. *Nucleosides Nucleotides Nucleic Acids* **31**, 277-285, doi:10.1080/15257770.2012.658131 (2012).

17 Molla, A. *et al.* Human serum attenuates the activity of protease inhibitors toward wild-type and mutant human immunodeficiency virus. *Virology* **250**, 255-262, doi:10.1006/viro.1998.9383 (1998).

18 Kawatkar, S. P. *et al.* Design and structure-activity relationships of novel inhibitors of human rhinovirus 3C protease. *Bioorg Med Chem Lett* **26**, 3248-3252, doi:10.1016/j.bmcl.2016.05.066 (2016).

19 Perron, M. *et al.* GS-5806 Inhibits a Broad Range of Respiratory Syncytial Virus Clinical Isolates by Blocking the Virus-Cell Fusion Process. *Antimicrob Agents Chemother* **60**, 1264-1273, doi:10.1128/AAC.01497-15 (2015).

20 Marty, F. M. *et al.* A Phase 2b, Randomized, Double-blind, Placebo-Controlled Multicenter Study Evaluating Antiviral Effects, Pharmacokinetics, Safety, and Tolerability of Presatovir in Hematopoietic Cell Transplant Recipients with Respiratory Syncytial Virus (RSV) Infection of the Lower Respiratory Tract. *Clin Infect Dis*, doi:10.1093/cid/ciz1167 (2019).

21 Nie, J. *et al.* Establishment and validation of a pseudovirus neutralization assay for SARS-CoV-2. *Emerg Microbes Infect* **9**, 680-686, doi:10.1080/22221751.2020.1743767 (2020).

22 Gordon, C. J. *et al.* Remdesivir is a direct-acting antiviral that inhibits RNA-dependent RNA polymerase from severe acute respiratory syndrome coronavirus 2 with high potency. *J Biol Chem* **295**, 6785-6797, doi:10.1074/jbc.RA120.013679 (2020).

23 Beigel, J. H. *et al.* Remdesivir for the Treatment of Covid-19 - Preliminary Report. *N Engl J Med*, doi:10.1056/NEJMoa2007764 (2020).

24 de Wit, E. *et al.* Prophylactic and therapeutic remdesivir (GS-5734) treatment in the rhesus macaque model of MERS-CoV infection. *Proc Natl Acad Sci U S A* **117**, 6771-6776, doi:10.1073/pnas.1922083117 (2020).

25 Williamson, B. N. *et al.* Clinical benefit of remdesivir in rhesus macaques infected with SARS-CoV-2. *bioRxiv* doi: https://doi.org/10.1101/2020.04.15.043166 (2020).

26 Sheahan, T. P. *et al.* Comparative therapeutic efficacy of remdesivir and combination lopinavir, ritonavir, and interferon beta against MERS-CoV. *Nat Commun* **11**, 222, doi:10.1038/s41467-019-13940-6 (2020).

27 Sheahan, T. P. *et al.* Broad-spectrum antiviral GS-5734 inhibits both epidemic and zoonotic coronaviruses. *Sci Transl Med* **9**, doi:10.1126/scitranslmed.aal3653 (2017).

28 Gao, J., Tian, Z. & Yang, X. Breakthrough: Chloroquine phosphate has shown apparent efficacy in treatment of COVID-19 associated pneumonia in clinical studies. *Biosci Trends* **14**, 72-73, doi:10.5582/bst.2020.01047 (2020).

29 Gautret, P. *et al.* Clinical and microbiological effect of a combination of hydroxychloroquine and azithromycin in 80 COVID-19 patients with at least a six-day follow up: A pilot observational study. *Travel Med Infect Dis* **34**, 101663, doi:10.1016/j.tmaid.2020.101663 (2020).

30 Molina, J. M. *et al.* No evidence of rapid antiviral clearance or clinical benefit with the combination of hydroxychloroquine and azithromycininpatients withsevereCOVID-19 infection. *Med Mal Infect* https://doi.org/10.1016/j.medmal.2020.03.006 (2020).

31 Rosenberg, E. S. *et al.* Association of Treatment With Hydroxychloroquine or Azithromycin With In-Hospital Mortality in Patients With COVID-19 in New York State. *JAMA*, doi:10.1001/jama.2020.8630 (2020).

32 Patick, A. K. *et al.* In vitro antiviral activity of AG7088, a potent inhibitor of human rhinovirus 3C protease. *Antimicrob Agents Chemother* **43**, 2444-2450 (1999).

33 Hayden, F. G. *et al.* Phase II, randomized, double-blind, placebo-controlled studies of ruprintrivir nasal spray 2-percent suspension for prevention and treatment of experimentally induced rhinovirus colds in healthy volunteers. *Antimicrob Agents Chemother* **47**, 3907-3916, doi:10.1128/aac.47.12.3907-3916.2003 (2003).

34 Copertino Jr., D. C. *et al.* Antiretroviral Drug Activity and Potential for Pre-Exposure Prophylaxis Against COVID-19 and HIV Infection. *ChemRxiv* https://doi.org/10.26434/chemrxiv.12250199.v1 (2020).

35 Elfiky, A. A. Ribavirin, Remdesivir, Sofosbuvir, Galidesivir, and Tenofovir against SARS-CoV-2 RNA dependent RNA polymerase (RdRp): A molecular docking study. *Life Sci* **253**, 117592, doi:10.1016/j.lfs.2020.117592 (2020).

36 Jácome, R., Campillo-Balderas, J. A., León, S. P. d., Becerra, A. & Lazcano, A. Sofosbuvir as a Potential Alternative to Treat the SARS-CoV-2 Epidemic. *Sci Rep* **10** (2020).

37 Izzi, A., Messina, V., Rinaldi, L. & Maggi, P. Editorial - Sofosbuvir/Velpatasvir as a Combination With Strong Potential Activity Against SARS-CoV2 (COVID-19) Infection: How to Use Direct-Acting Antivirals as Broad-Spectrum Antiviral Agents. *Eur Rev Med Pharmacol Sci* **24**, 5193-5194 (2020).

38 Chien, M. *et al.* Nucleotide Analogues as Inhibitors of SARS-CoV-2 Polymerase. *bioRxiv* doi: 10.1101/2020.03.18.997585 (2020).

39 Siegel, D. *et al.* Discovery and Synthesis of a Phosphoramidate Prodrug of a Pyrrolo[2,1-f][triazin-4-amino] Adenine C-Nucleoside (GS-5734) for the Treatment of Ebola and Emerging Viruses. *J Med Chem* **60**, 1648-1661, doi:10.1021/acs.jmedchem.6b01594 (2017).

40 Cho, A. *et al.* Discovery of the first C-nucleoside HCV polymerase inhibitor (GS-6620) with demonstrated antiviral response in HCV infected patients. *J Med Chem* **57**, 1812-1825, doi:10.1021/jm400201a (2014).

41 Carroll, S. S. *et al.* Robust antiviral efficacy upon administration of a nucleoside analog to hepatitis C virus-infected chimpanzees. *Antimicrob Agents Chemother* **53**, 926-934, doi:10.1128/AAC.01032-08 (2009).

42 Sofia, M. J. Nucleotide prodrugs for HCV therapy. *Antivir Chem Chemother* **22**, 23-49, doi:10.3851/IMP1797 (2011).

43 Deval, J. *et al.* Molecular Basis for the Selective Inhibition of Respiratory Syncytial Virus RNA Polymerase by 2'-Fluoro-4'-Chloromethyl-Cytidine Triphosphate. *PLoS Pathog* **11**, e1004995, doi:10.1371/journal.ppat.1004995 (2015).

44 Langley, D. R. *et al.* Inhibition of hepatitis B virus polymerase by entecavir. *J Virol* **81**, 3992-4001, doi:10.1128/JVI.02395-06 (2007).

45 De Clercq, E. Clinical potential of the acyclic nucleoside phosphonates cidofovir, adefovir, and tenofovir in treatment of DNA virus and retrovirus infections. *Clin Microbiol Rev* **16**, 569-596, doi:10.1128/cmr.16.4.569-596.2003 (2003).

46 Vanderlinden, E. *et al.* Distinct Effects of T-705 (Favipiravir) and Ribavirin on Influenza Virus Replication and Viral RNA Synthesis. *Antimicrob Agents Chemother* **60**, 6679-6691, doi:10.1128/AAC.01156-16 (2016).

47 Eron, J. J. *et al.* Once-daily versus twice-daily lopinavir/ritonavir in antiretroviral-naive HIV-positive patients: a 48-week randomized clinical trial. *J Infect Dis* **189**, 265-272, doi:10.1086/380799 (2004).

48 Zhu, L. *et al.* Pharmacokinetics and inhibitory quotient of atazanavir/ritonavir versus lopinavir/ritonavir in HIV-infected, treatment-naive patients who participated in the CASTLE Study. *J Antimicrob Chemother* **67**, 465-468, doi:10.1093/jac/dkr490 (2012).

49 Sadler, B. M. & Stein, D. S. Clinical pharmacology and pharmacokinetics of amprenavir. *Ann Pharmacother* **36**, 102-118, doi:10.1345/aph.10423 (2002).

50 Bardsley-Elliot, A. & Plosker, G. L. Nelfinavir: an update on its use in HIV infection. *Drugs* **59**, 581-620, doi:10.2165/00003495-200059030-00014 (2000).

51 Lea, A. P. & Faulds, D. Ritonavir. *Drugs* **52**, 541-546; discussion 547-548, doi:10.2165/00003495-199652040-00007 (1996).

52 Zeldin, R. K. & Petruschke, R. A. Pharmacological and therapeutic properties of ritonavir-boosted protease inhibitor therapy in HIV-infected patients. *J Antimicrob Chemother* **53**, 4-9, doi:10.1093/jac/dkh029 (2004).

53 Stein, D. S. *et al.* A 24-week open-label phase I/II evaluation of the HIV protease inhibitor MK-639 (indinavir). *AIDS* **10**, 485-492, doi:10.1097/00002030-199605000-00006 (1996).

54 Anderson, P. L. *et al.* Indinavir plasma protein binding in HIV-1-infected adults. *AIDS* **14**, 2293-2297, doi:10.1097/00002030-200010200-00010 (2000).

55 Singh, K. *et al.* Pharmacokinetics and safety of saquinavir/ritonavir and omeprazole in HIV-infected subjects. *Clin Pharmacol Ther* **83**, 867-872, doi:10.1038/sj.clpt.6100375 (2008).

56 Surleraux, D. L. *et al.* Discovery and selection of TMC114, a next generation HIV-1 protease inhibitor. *J Med Chem* **48**, 1813-1822, doi:10.1021/jm049560p (2005).

57 MacGregor, T. R. *et al.* Pharmacokinetic characterization of different dose combinations of coadministered tipranavir and ritonavir in healthy volunteers. *HIV Clin Trials* **5**, 371-382, doi:10.1310/RRX7-49ME-27V7-MWWV (2004).

58 Saag, M. S. *et al.* Efficacy and safety of emtricitabine vs stavudine in combination therapy in antiretroviral-naive patients: a randomized trial. *JAMA* **292**, 180-189, doi:10.1001/jama.292.2.180 (2004).

59 Custodio, J. M. *et al.* Pharmacokinetics and Safety of Tenofovir Alafenamide in HIV-Uninfected Subjects with Severe Renal Impairment. *Antimicrob Agents Chemother* **60**, 5135-5140, doi:10.1128/AAC.00005-16 (2016).

60 Ruane, P. J. *et al.* Antiviral activity, safety, and pharmacokinetics/pharmacodynamics of tenofovir alafenamide as 10-day monotherapy in HIV-1-positive adults. *J Acquir Immune Defic Syndr* **63**, 449-455, doi:10.1097/QAI.0b013e3182965d45 (2013).

61 Ray, A. S. *et al.* Intracellular metabolism of the nucleotide prodrug GS-9131, a potent anti-human immunodeficiency virus agent. *Antimicrob Agents Chemother* **52**, 648-654, doi:10.1128/AAC.01209-07 (2008).

62 Goebel, F. *et al.* Short-term antiviral activity of TMC278--a novel NNRTI--in treatment-naive HIV-1-infected subjects. *AIDS* **20**, 1721-1726, doi:10.1097/01.aids.0000242818.65215.bd (2006).

63 Adkins, J. C. & Noble, S. Efavirenz. *Drugs* **56**, 1055-1064; discussion 1065-1056, doi:10.2165/00003495-199856060-00014 (1998).

64 Gallant, J. E. *et al.* Antiviral Activity, Safety, and Pharmacokinetics of Bictegravir as 10-Day Monotherapy in HIV-1-Infected Adults. *J Acquir Immune Defic Syndr* **75**, 61-66, doi:10.1097/QAI.0000000000001306 (2017).

65 Sheng, X. C. *et al.* Discovery of GS-9256: a novel phosphinic acid derived inhibitor of the hepatitis C virus NS3/4A protease with potent clinical activity. *Bioorg Med Chem Lett* **22**, 1394-1396, doi:10.1016/j.bmcl.2011.12.038 (2012).

66 Yang, H. *et al.* Preclinical characterization of the novel hepatitis C virus NS3 protease inhibitor GS-9451. *Antimicrob Agents Chemother* **58**, 647-653, doi:10.1128/AAC.00487-13 (2014).

67 Taylor, J. G. *et al.* Discovery of the pan-genotypic hepatitis C virus NS3/4A protease inhibitor voxilaprevir (GS-9857): A component of Vosevi((R)). *Bioorg Med Chem Lett* **29**, 2428-2436, doi:10.1016/j.bmcl.2019.03.037 (2019).

68 Shih, I. H. *et al.* Mechanistic characterization of GS-9190 (Tegobuvir), a novel nonnucleoside inhibitor of hepatitis C virus NS5B polymerase. *Antimicrob Agents Chemother* **55**, 4196-4203, doi:10.1128/AAC.00307-11 (2011).

69 Lazerwith, S. E. *et al.* Discovery of GS-9669, a thumb site II non-nucleoside inhibitor of NS5B for the treatment of genotype 1 chronic hepatitis C infection. *J Med Chem* **57**, 1893-1901, doi:10.1021/jm401420j (2014).

70 Link, J. O. *et al.* Discovery of ledipasvir (GS-5885): a potent, once-daily oral NS5A inhibitor for the treatment of hepatitis C virus infection. *J Med Chem* **57**, 2033-2046, doi:10.1021/jm401499g (2014).

71 Link, J. O. *et al.* Discovery of velpatasvir (GS-5816): A potent pan-genotypic HCV NS5A inhibitor in the single-tablet regimens Vosevi((R)) and Epclusa((R)). *Bioorg Med Chem Lett* **29**, 2415-2427, doi:10.1016/j.bmcl.2019.04.027 (2019).

72 Xu, J., Shi, P. Y., Li, H. & Zhou, J. Broad Spectrum Antiviral Agent Niclosamide and Its Therapeutic Potential. *ACS Infect Dis* **6**, 909-915, doi:10.1021/acsinfecdis.0c00052 (2020).

73 Takano, T., Katoh, Y., Doki, T. & Hohdatsu, T. Effect of chloroquine on feline infectious peritonitis virus infection in vitro and in vivo. *Antiviral Res* **99**, 100-107, doi:10.1016/j.antiviral.2013.04.016 (2013).

74 Xu, L. *et al.* Cobicistat (GS-9350): A Potent and Selective Inhibitor of Human CYP3A as a Novel Pharmacoenhancer. *ACS Med Chem Lett* **1**, 209-213, doi:10.1021/ml1000257 (2010).

75 Takahashi, K. *et al.* In vitro and in vivo activities of T-705 and oseltamivir against influenza virus. *Antivir Chem Chemother* **14**, 235-241, doi:10.1177/095632020301400502 (2003).

76 Noshi, T. *et al.* In vitro characterization of baloxavir acid, a first-in-class cap-dependent endonuclease inhibitor of the influenza virus polymerase PA subunit. *Antiviral Res* **160**, 109-117, doi:10.1016/j.antiviral.2018.10.008 (2018).

77 Ratziu, V. *et al.* A phase 2, randomized, double-blind, placebo-controlled study of GS-9450 in subjects with nonalcoholic steatohepatitis. *Hepatology* **55**, 419-428, doi:10.1002/hep.24747 (2012).

78 Bond, D. A. & Woyach, J. A. Targeting BTK in CLL: Beyond Ibrutinib. *Curr Hematol Malig Rep* **14**, 197-205, doi:10.1007/s11899-019-00512-0 (2019).

79 Mossel, E. C. *et al.* Exogenous ACE2 expression allows refractory cell lines to support severe acute respiratory syndrome coronavirus replication. *J Virol* **79**, 3846-3850, doi:10.1128/JVI.79.6.3846-3850.2005 (2005).

80 Xie, X. *et al.* An infectious cDNA clone of SARS-CoV-2. *Cell Host Microbe*, doi:10.1016/j.chom.2020.04.004 (2020).

Table 1. Nucleoside and nucleotide analogs against SARS-CoV-2-Nluc

Compound name	EC_{50} (μM)[a]	CC_{50} (μM)[a]	SI[b]	Nucleoside/tide analog	Reference
Remdesivir (GS-5734)	0.115 ± 0.007	32.7 ± 5.2	284	1'-CN-C-adenosine	39
GS-6620	>10	>50	-	1'CN, 2'Me-C-adenosine	40
MK-0608	>10	>50	-	2'Me-7-deaza-adenosine	41
PSI-352938	>10	>50	-	2'Me-2'F-guanosine	42
Sofosbuvir	>10	>50	-	2'Me, 2'F-uridine	16
ALS-8112	>10	>50	-	2'F, 4'Cl-Me-cytidine	43
Entecavir	>10	>50	-	Carbocyclic deoxyguanosine	44
Cidofovir	>10	>50	-	Acyclic cytidine phosphonate	45
Favipiravir (T-705)	>10	>50	-	Modified nucleobase	46
Ribavirin	>10	>50	-	Ribofuranosyl	-

[a]Values are mean ± standard deviation of two independent replicate experiments in A549-hACE2 cells

[b]Selectivity index (SI) = CC_{50} / EC_{50}

518 **Table 2. HIV drugs against SARS-CoV-2-Nluc**
519

Inhibitor class	Compound name	EC_{50} (μM)[a]	CC_{50} (μM)[a]	SI[b]	Exposure (μM)[c]	Plasma protein binding (%)[d]	Reference
HIV protease (aspartyl)	Lopinavir	9.00 ± 0.42	31.5 ± 2.5	3.5	15.6 / 8.8	98-99	[47, 48]
	Amprenavir	>10	>50	-	-	90	[49]
	Nelfinavir	0.77 ± 0.32	12.0 ± 1.3	15.7	8.3 / 2.6	>98	[50, e]
	Ritonavir	>10	36.9 ± 1.7	-	-	98-99	[51, 52]
	Indinavir	>10	>50	-	-	61	[53, 54]
	Saquinavir	8.95 ± 0.31	35.1 ± 11.7	3.9	3.7 / 0.65	98	[55, e]
	Darunavir	>10	>50	-	-	95	[56, e]
	Atazanavir	>10	>50	-	-	86	[48]
	Tipranavir	8.65 ± 0.16	28.4 ± 0.5	3.3	130 / 30.8	99.9	[57]
HIV NRTI	Emtricitabine (FTC)	>10	>50	-	C_{max} 7.9	4	[58, e]
	Tenofovir alafenamide (TAF)	>10	>50	-	C_{max} 0.4	80	[59, 60]
	Rovafovir (GS-9131)	>10	>50	-	-	-	[61]
HIV NNRTI	Rilpivirine	7.80 ± 1.04	14.6 ± 1.6	1.9	0.83 / 0.30	99.7	[62, e]
	Efavirenz	>9.6	37.6 ± 10.7	<3.9	12.9 / 5.6	99.5-99.8	[63]
HIV integrase	Bictegravir[f]	>10	>50	-	-	>99	[64]

520
521 [a]Values are mean ± standard deviation of two independent replicates in A549-hACE2 cells
522 [b]SI = CC_{50} / EC_{50}
523 [c]Values represent C_{max} / C_{min} for human exposures in the clinic based on approved dosing
524 schedules
525 [d]Data from literature as cited
526 [e]Information from product description

527 **Table 3. HCV drugs against SARS-CoV-2-Nluc**
528

Inhibitor class	Compound name	EC_{50} (μM)[a]	CC_{50} (μM)[a]	Reference
HCV protease (serine)	GS-9256	>10	31.8 ± 10.9	65
	GS-9451	>10	>50	66
	Voxilaprevir	>10	16.0 ± 1.2	67
HCV nucleoside RdRp	Sofosbuvir	>10	>50	16
HCV non-nucleoside RdRp	GS-9130	>10	>50	-
	Tegobuvir	>10	17.9 ± 3.1	68
	Radalbuvir	>10	>50	69
HCV NS5A	Ledapisvir	>10	>50	70
	Velpatasvir	>10	>50	71

529
530 [a]Values are mean ± standard deviation of two independent replicates in A549-hACE2 cells

Table 4. Other drug classes against SARS-CoV-2-Nluc

Inhibitor class	Compound name	EC_{50} (μM)[a]	CC_{50} (μM)[a]	SI[b]	Reference
HRV protease (serine)	Rupintrivir	1.87 ± 0.47	>50	>26.7	[18]
Antihelminthic	Niclosamide	0.715 ± 0.332	1.28 ± 0.23	1.8	[72]
Antimalarial / amebicide	Chloroquine	1.32 ± 0.36	>50	>37.9	[73]
RSV fusion	Presatovir	2.53 ± 0.69	34.0 ± 6.5	13.5	[19]
CYP3A inhibitor	Cobicistat	2.74 ± 0.20	47.3 ± 2.5	17.3	[74]
Influenza neuraminidase	Oseltamivir carboxylate	>10	>50	-	[75]
Influenza endonuclease	Baloxavir	>10	47.0 ± 1.3	-	[76]
Caspases 1, 8, & 9	Nivocasan (GS-9450)	>10	>50	-	[77]
BTK	Tirabrutinib	>10	>50	-	[78]
	Ibrutinib[j]	>10	>50	-	[78]

[a]Values are mean ± standard deviation of two independent replicates in A549-hACE2 cells

[b]SI = CC_{50} / EC_{50}

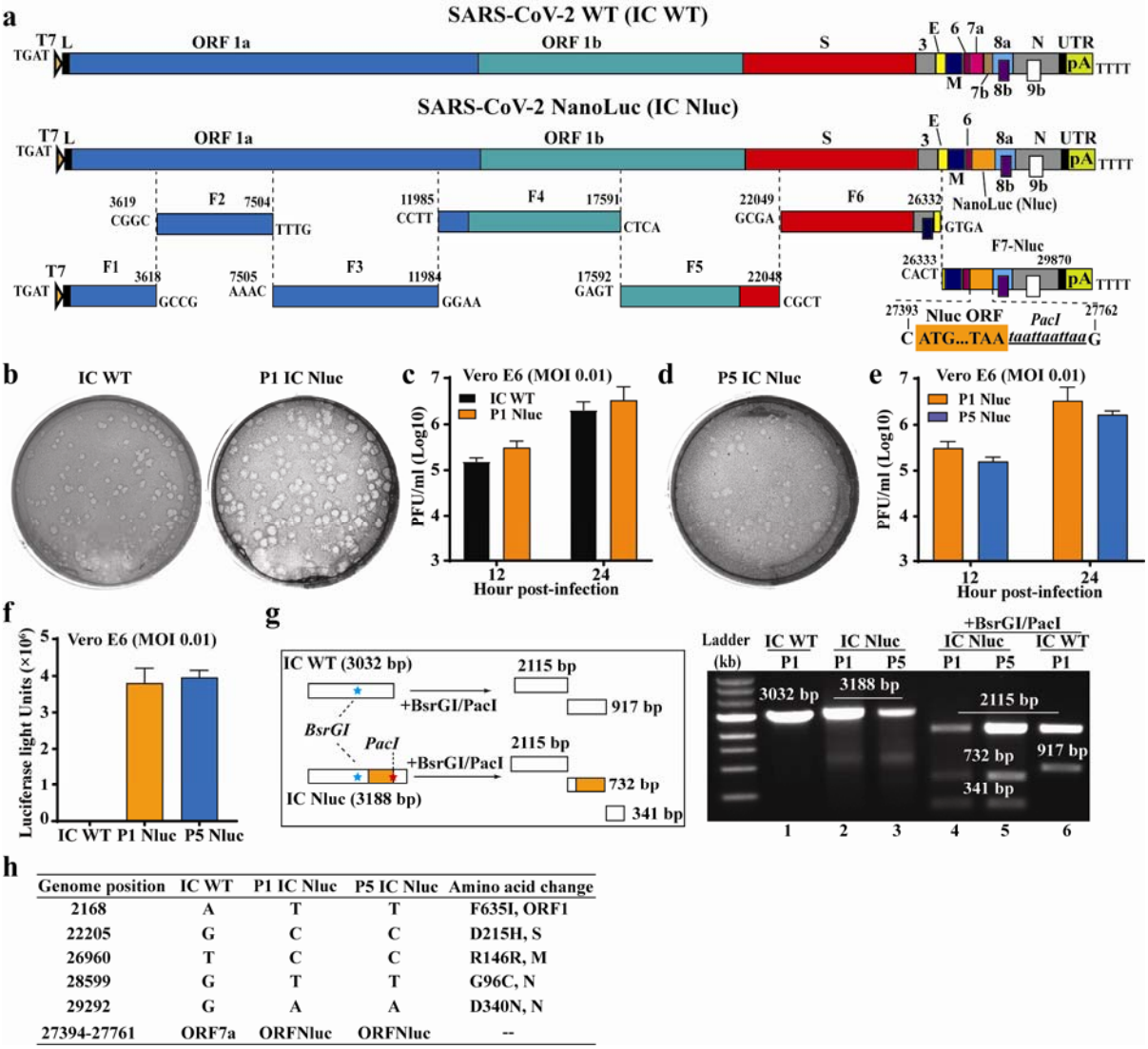

Genome position	IC WT	P1 IC Nluc	P5 IC Nluc	Amino acid change
2168	A	T	T	F635I, ORF1
22205	G	C	C	D215H, S
26960	T	C	C	R146R, M
28599	G	T	T	G96C, N
29292	G	A	A	D340N, N
27394-27761	ORF7a	ORFNluc	ORFNluc	--

Figure 1. Development and characterization of SARS-CoV-2-Nluc. (a) Assembly of the full-length SARS-CoV-2-Nluc cDNA. The Nanoluciferase (Nluc) gene together with a *PacI* site was placed downstream of the regulatory sequence of ORF7 to replace the ORF7 sequence. The nucleotide identities of the Nluc substitution sites are indicated. (b) Plaque morphologies of infectious clone derived P1 SARS-CoV-2-Nluc (P1 IC Nluc) and wild-type SARS-CoV-2 (IC WT). (c) Replication kinetics. Vero E6 cells were infected with infectious clone derived IC WT or P1 IC Nluc at MOI 0.01. Viruses in culture supernatants were quantified by plaque assay. (d) Plaque morphology of P5 IC Nluc. (e) Replication kinetics of P5 IC Nluc on Vero E6 cells. (f) Luciferase signals produced from SARS-CoV-2-Nluc-infected Vero E6 cells at 12 h post-

infection. Cells were infected with viruses at MOI 0.1. (g) Gel analysis of IC Nluc virus stability. The left panel depicts the theoretical results of RT-PCR followed by restriction enzyme digestion. The right panel shows the gel analysis of the RT-PCR products before (lanes 1–3) and after BsrGI/PacI digestion (lanes 4–6). (h) Summary of full-genome sequences of P1 and P5 IC Nluc viruses. Nucleotide and amino acid differences from the IC WT are indicated.

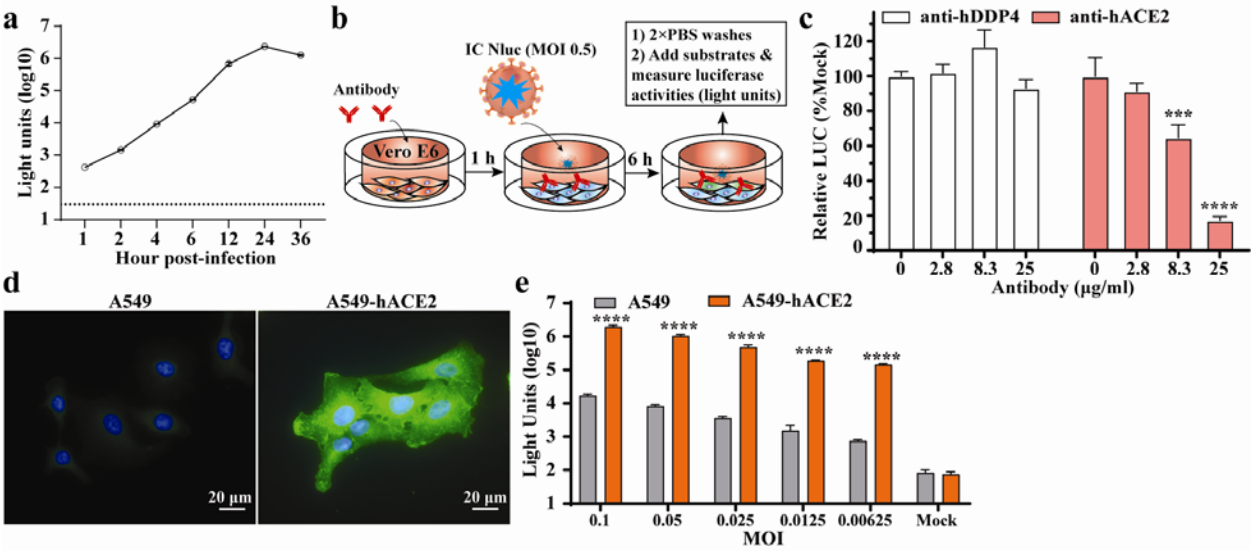

Figure 2. Application of SARS-CoV-2-Nluc in analyzing hACE2 as an entry receptor. (a) Replication kinetics of SARS-CoV-2-Nluc (IC Nluc) on Vero E6 cells. Cells were infected with IC Nluc at MOI 1.0. At given time points, cells were harvested for luciferase signal measurement. The means and standard deviations from three independent experiments are presented. (b) Diagram to analyze hACE2 for IC Nluc entry. (c) Relative luciferase signals following infection of cells that were preincubated with anti-hDPP4 or anti-hACE2 antibodies. The luciferase signals from antibody-treated groups were normalized to those from untreated groups. The average and standard deviation of three independent experiments are presented. (d) Immunofluorescence analysis of hACE2 expression in A549-hACE2 cells. At 24 h post-seeding, the cells were fixed and stained with anti-hACE2 polyclonal antibody. (e) Luciferase signals from IC Nluc infected-A549 and A549-hACE2 cells. Cells were infected with indicated MOIs and luciferase signals were measured at 24 h post-infection.

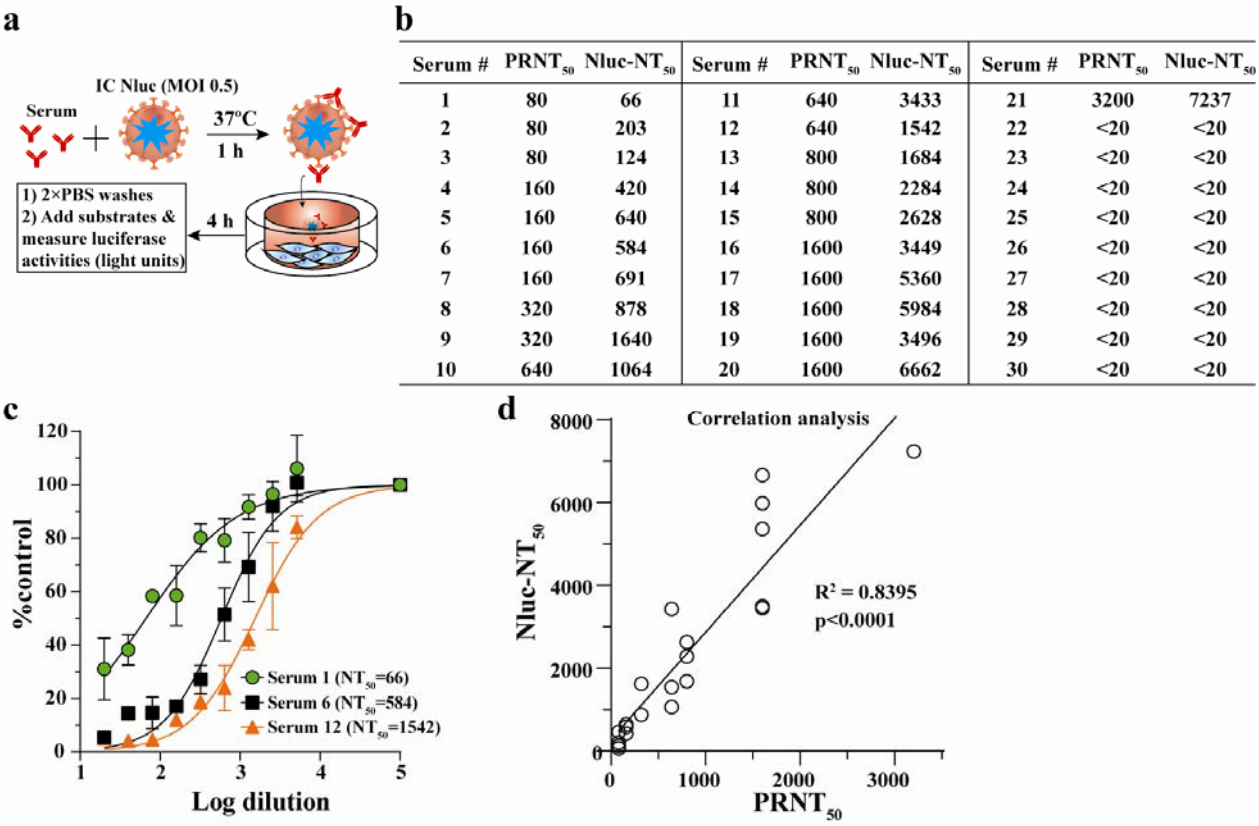

Serum #	PRNT$_{50}$	Nluc-NT$_{50}$	Serum #	PRNT$_{50}$	Nluc-NT$_{50}$	Serum #	PRNT$_{50}$	Nluc-NT$_{50}$
1	80	66	11	640	3433	21	3200	7237
2	80	203	12	640	1542	22	<20	<20
3	80	124	13	800	1684	23	<20	<20
4	160	420	14	800	2284	24	<20	<20
5	160	640	15	800	2628	25	<20	<20
6	160	584	16	1600	3449	26	<20	<20
7	160	691	17	1600	5360	27	<20	<20
8	320	878	18	1600	5984	28	<20	<20
9	320	1640	19	1600	3496	29	<20	<20
10	640	1064	20	1600	6662	30	<20	<20

Figure 3. A rapid SARS-CoV-2-Nluc-based neutralization assay. (a) Schematic of the rapid neutralization assay. (b) Summary of neutralizing titers as measured by PRNT and SARS-CoV-2-Nluc neutralization (Nluc-NT) assay. Serum specimens 1-21 were from COVID-19 patients with confirmed prior RT-PCR diagnosis. Serum specimens 22-30 were from non-COVID-19 individuals. (c) Representative neutralizing curves of the Nluc-NT assay. The means and standard deviations from two independent experiments are shown. (d) Correlation analysis between the Nluc-NT$_{50}$ and PRNT$_{50}$ values. The correlation efficiency R^2 and p value calculated from a linear regression analysis are shown.

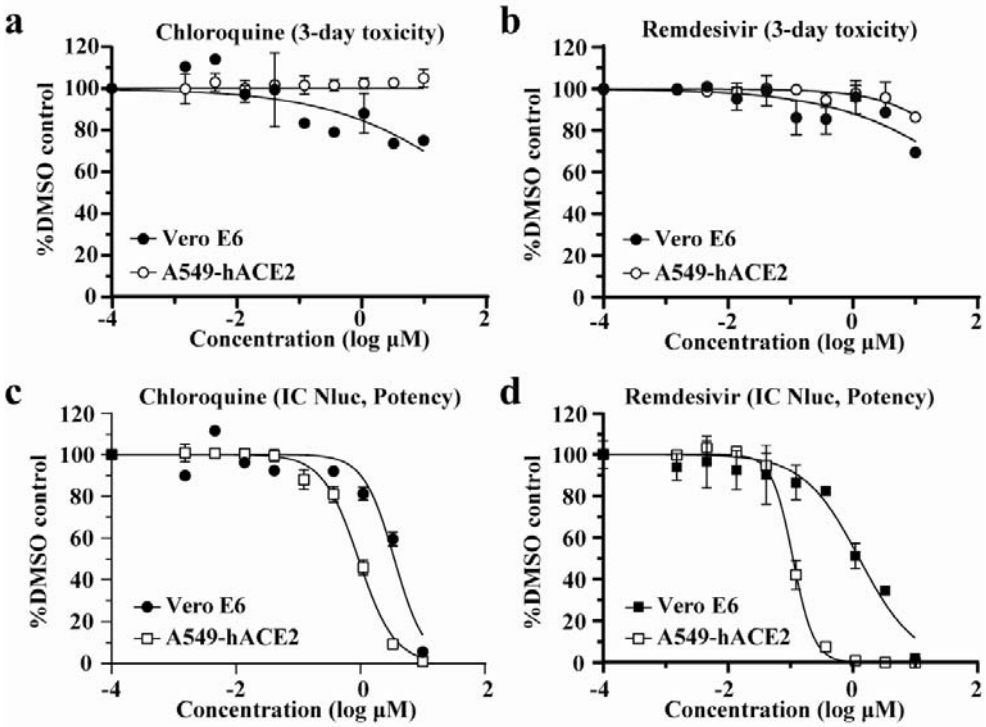

e

Compound	3-day CC_{50} (μM)		EC_{50} (μM)		Selectivity index (SI)	
	Vero E6	A549-hACE2	Vero E6	A549-hACE2	Vero E6	A549-hACE2
Chloroquine	>50	>50	3.52 ± 0.35	1.32 ± 0.06	>14	>38
Remdesivir	>50	32.7 ± 5.2	1.28 ± 0.25	0.115 ± 0.007	>39	284

Figure 4. SARS-CoV-2-Nluc-based antiviral screening. A three-day cytotoxicity assay was performed for chloroquine (a) and remdesivir (b) on Vero E6 and A549-hACE2 cells. A two-day SARS-CoV-2-Nluc infection assay (MOI 0.025) was performed to estimate the EC_{50} values of chloroquine (c) and remdesivir (d) on Vero E6 and A549-hACE2 cells. (e) Summary of CC_{50}, $EC_{50,}$ and selectivity index (SI).

Methods

Cell lines

African green monkey kidney epithelial cells Vero E6 (ATCC®CRL-1586) were purchased from the American Type Culture Collection (ATCC, Bethesda, MD) and maintained in a high-glucose Dulbecco's modified Eagle's medium (DMEM) supplemented with 10% fetal bovine serum (FBS; HyClone Laboratories, South Logan, UT) and 1% penicillin/streptomycin (P/S). Human alveolar epithelial cell line (A549) and human embryonic kidney cells (HEK293) were maintained in a high-glucose DMEM supplemented with 10% fetal bovine serum, 1% P/S and 1% HEPES (ThermoFisher Scientific). The A549-hACE2 and HEK293-hACE2 cells that stably express human angiotensin-converting enzyme 2 (hACE2)[79] were grown in the culture medium supplemented with 10 µg/mL Blasticidin S. Cells were grown at 37°C with 5% CO_2. All culture medium and antibiotics were purchased from ThermoFisher Scientific (Waltham, MA). All cell lines were tested negative for mycoplasma.

Generation of SARS-CoV-2-Nluc

A subclone (F7-Nluc) was constructed by substituting the ORF7 of the viral genome with the reporter Nano^{R}luciferase gene followed by a PacI restriction site (taattaattaa). All subclones were validated by Sanger sequencing prior to assembling the full-length clone. The full-length infectious cDNA clone of SARS-CoV-2-Nluc was generated by *in vitro* ligation of seven contiguous panel of cDNA according to a protocol as reported previously[80]. RNA transcript was *in vitro* synthesized by the mMESSAGE mMACHINE™ T7 Transcription Kit (ThermoFisher Scientific) and electroporated into Vero E6 cells to recover the recombinant SARS-CoV-2-Nluc by using the same protocol as described reviously[80]. The viral stock was prepared by amplifying the SARS-CoV-2-Nluc on Vero E6 cells for one round (P1). The titer of the virus stock was determined by a standard plaque assay. All SARS-CoV-2-Nluc propagation and other virus-related work were performed at the BSL-3 facility at UTMB.

603 **RNA extraction, RT-PCR and Sanger sequencing**

604 250 µL of culture fluids were mixed with three volume of TRIzol™ LS Reagent (Thermo Fisher
605 Scientific). Viral RNAs were extracted per manufacturer's instructions. The extracted RNAs
606 were dissolved in 30 µL nuclease-free water. 11 µL RNA samples were used for reverse
607 transcription by using the SuperScript™ IV First-Strand Synthesis System (ThermoFisher
608 Scientific) with random hexamer primers. Nine DNA fragments flanking the entire viral genome
609 were amplified by PCR with specific primers. The resulting DNAs were cleaned up by the
610 QIAquick PCR Purification Kit, and the genome sequences were determined by Sanger
611 sequencing at GENEWIZ (South Plainfield, NJ).

612 **hACE2 antibody blocking assay**

613 15,000 Vero E6 cells per well were seeded in a white opaque 96-well plate (Corning). On the
614 next day, cells were wash three times with PBS to remove any residual FBS and followed by 1-
615 hour treatment with goat anti-human ACE2 antibody (R&D Systems) or anti-hDDP4 antibody
616 (R&D Systems) (both antibodies were prepared in OptiMEM medium to the given
617 concentrations). Afterwards, cells were infected with SARS-CoV-2-Nluc (MOI 0.5). At 6h post-
618 infection, cells were washes twice and followed by the addition of 50 µL Nano luciferase
619 substrate (Promega). After 5 minutes of incubation at room temperature, luciferase signals were
620 measured using a Synergy™ Neo2 microplate reader (BioTek) per the manufacturer's
621 instructions.

622 **Immunofluorescence Assay**

623 Cells were seeded on a 4-well chamber slide. At 24 h post-seeding, cells were fixed and
624 permeabilized with 0.1% Triton X-100. After 1 h-blocking with PBS+1% FBS, cellular hACE2
625 was probed firstly by goat anti-human ACE2 antibody (R&D Systems). After three times of PBS
626 washes, the cells were incubated with donkey anti-goat IgG conjugated with Alexa Fluor® 488

(ThermoFisher Scientific). Finally, the fluorescence images were acquired using the Nikon Ti2-E inverted microscope armed with a 60× objective.

SARS-CoV-2-Nluc neutralization assay

Vero E6 cells (15,000 per well in medium containing 2% FBS) were plated into a white opaque 96-well plate (Corning). At 16 h post-seeding, 30 µL of 2-fold serial diluted human sera were mixed with 30 µL of SARS-CoV-2-Nluc (MOI 0.5) and incubated at 37°C for 1 hour. Afterwards, 50 µL of virus-sera complexes were transferred to each well of the 96-well plate. After 4 h of incubation at 37°C 5% CO_2, cells were washed twice followed by the addition of Nano luciferase substrate (Promega). Luciferase signals were measured using a Synergy™ Neo2 microplate reader (BioTek) per the manufacturer's instructions. The relative luciferase signal was calculated by normalizing the luciferase signals of serum-treated groups to those of the no-serum controls. The concentration that reduces the 50% luciferase signal (NT_{50}) were estimated by using a four-parameter logistic regression model from the Prism 8 software (GraphPad Software Inc., San Diego CA).

Plaque reduction neutralization test (PRNT)

Approximately 1.2×10^6 Vero E6 cells were seeded to each well of 6-well plates. On the following day, 100 PFU of infectious clone-derived wild-type SARS-CoV-2 was incubated with serially diluted serum (total volume of 200 µL) at 37°C for 1 h. The virus-serum mixture was transferred to the pre-seeded Vero E6 cells in 6-well plate. After incubation at 37°C for 1 h, 2 mL of 2% high gel temperature agar (SeaKem) in DMEM with 5% FBS and 1% P/S was added to the infected cells per well. After 2-day incubation, 2 ml of neutral red (1 g/L in PBS; Sigma) was added to the agar-covered cells. After another 5-h incubation, neutral red was removed, and individual plaques were counted for NT_{50} calculation. Each specimen was tested in duplicates.

SARS-CoV-2-Nluc antiviral assay

Vero or A549-hACE2 cells (12,000 cells per well in phenol-red free medium containing 2% FBS) were plated into a white opaque 96-well plate (Corning). On the next day, 2-fold serial dilutions of compounds were prepared in DMSO. The compounds were further diluted 100-fold in the phenol-red free culture medium containing 2% FBS. Cell culture fluids were removed and incubated with 50 µL of diluted compound solutions and 50 µL of SARS-CoV2-Nluc viruses (MOI 0.025). At 48 h post-infection, 50 µL Nano luciferase substrates (Promega) were added to each well. Luciferase signals were measured using a Synergy™ Neo2 microplate reader. The relative luciferase signals were calculated by normalizing the luciferase signals of the compound-treated groups to that of the DMSO-treated groups (set as 100%). The relative luciferase signal (Y axis) versus the $\log_{10}$ values of compound concentration (X axis) was plotted in software Prism 8. The EC_{50} (compound concentration for reducing 50% of luciferase signal) were calculated using a nonlinear regression model (four parameters). Two experiments were performed with technical duplicates.

Cytotoxicity assay

Vero or A549-hACE2 cells (5,000 cells per well in phenol-red free medium containing 2% FBS) were plated into a clear flat bottom 96-well plate (Nunc). On the next day, 2-fold serial dilutions of compounds were prepared in DMSO. The compounds were further diluted 100-fold. 50 µL diluted compound solutions were added to each well of the cell plates. At 72 h post-treatment, 4 µL of Cell Counting Kit-8 (CCK-8; Sigma-Aldrich) was added to each well. After incubation at 37°C for 90 min, absorbance at 450 nm was measured using the Cytation5 multi-mode microplate reader (BioTek). The relative cell viability was calculated by normalizing the absorbance of the compound-treated groups to that of the DMSO-treated groups (set as 100%). The relative cell viability (Y axis) versus the $\log_{10}$ values of compound concentration (X axis) were plotted in software Prism 8. The CC_{50} (compound concentration for reducing 50% of cell

675 viability) were calculated using a nonlinear regression model (four parameters). Two
676 experiments were performed with technical duplicates.

677

678 **Acknowledgements**

679 We also thank colleagues at UTMB for support and discussions. A.E.M. is supported by
680 a Clinical and Translational Science Award NRSA (TL1) Training Core (TL1TR001440) from
681 NIH. C.R.F.-G. is supported by the predoctoral fellowship from the McLaughlin Fellowship
682 Endowment at UTMB. S.M. was supported by NIH grants AI114657 and AI146081. V.D.M. was
683 supported by NIH grants U19AI100625, R00AG049092, R24AI120942, and STARs Award from
684 the University of Texas System. P.-Y.S. was supported by NIH grants AI142759, AI134907,
685 AI145617, and UL1TR001439, and awards from the Sealy & Smith Foundation, Kleberg
686 Foundation, John S. Dunn Foundation, Amon G. Carter Foundation, Gilson Longenbaugh
687 Foundation, and Summerfield Robert Foundation.

688

689 **Author contributions**

690 X.X., T.C., V.D.M., J.P.B., and P.-Y.S conceived the study. X.X., A.E.M., X.Z., K.G.L.,
691 C.R.F.-G., J.Z., J.L., M.B., and J.P.B. performed the experiments. X.X., A.E.M., T.C., V.D.M.,
692 J.P.B., and P.-Y.S. analyzed the results. P.R. prepared the serum specimens. C.-T.K.T. and
693 S.M. provided critical reagents. X.X., M.B., T.C., J.P.B, and P.-Y.S wrote the manuscript.

694

695 **Competing interests**

696 UTMB has filed a patent on the reverse genetic system and reporter SARS-CoV-2. The
697 authors affiliated with Gilead Sciences, Inc. are employees of the company and own company
698 stock.